

RESEARCH ARTICLE | AUGUST 30 2023

Theory of singlet fission in carotenoid dimers

William Barford ; Cameron A. Chambers 



J. Chem. Phys. 159, 084116 (2023)

<https://doi.org/10.1063/5.0155476>



CrossMark

Articles You May Be Interested In

Two-photon absorption spectra of carotenoids compounds

J. Appl. Phys. (May 2011)

Extraction and identification of carotenoids from the skin of banana kepok (*Musa paradisiaca* L.)

AIP Conference Proceedings (April 2023)

Shifts of the $^1A_g \rightarrow ^1B_u$ electronic absorption of carotenoids in nonpolar and polar solvents

J. Chem. Phys. (October 1994)

500 kHz or 8.5 GHz?
And all the ranges in between.

Lock-in Amplifiers for your periodic signal measurements



Find out more



Theory of singlet fission in carotenoid dimers

Cite as: J. Chem. Phys. 159, 084116 (2023); doi: 10.1063/5.0155476

Submitted: 20 April 2023 • Accepted: 3 July 2023 •

Published Online: 30 August 2023



William Barford^{1,2,a)} and Cameron A. Chambers^{1,3}

AFFILIATIONS

¹ Department of Chemistry, Physical and Theoretical Chemistry Laboratory, University of Oxford, Oxford, OX1 3QZ, United Kingdom

² Balliol College, University of Oxford, Oxford, OX1 3BJ, United Kingdom

³ Lincoln College, University of Oxford, Oxford, OX1 3DR, United Kingdom

^{a)} Author to whom correspondence should be addressed: william.barford@chem.ox.ac.uk

ABSTRACT

We develop a theory of singlet fission in carotenoid dimers. Following photoexcitation of the “bright” state (i.e., a singlet electron–hole pair) in a single carotenoid, the first step in the singlet fission process is ultrafast intramolecular conversion into the highly correlated “dark” (or $2A_g$) state. This state has both entangled singlet triplet-pair and charge-transfer character. Our theory is predicated on the assumption that it is the singlet triplet-pair component of the “dark” state that undergoes bimolecular singlet fission. We use valence bond theory to develop a minimal two-chain model of the triplet-pair states. The single and double chain triplet-pair spectra are described, as this helps explain the dynamics and the equilibrated populations. We simulate the dynamics of the initial entangled pair state using the quantum Liouville equation, including both spin-conserving and spin-nonconserving dephasing processes. By computing the intrachain and interchain singlet, triplet, and quintet triplet-pair populations, we show that singlet fission critically depends on the interchain coupling and the driving potential (that determines endothermic vs exothermic fission).

© 2023 Author(s). All article content, except where otherwise noted, is licensed under a Creative Commons Attribution (CC BY) license (<http://creativecommons.org/licenses/by/4.0/>). <https://doi.org/10.1063/5.0155476>

I. INTRODUCTION

Singlet fission is a photophysical process whereby a photoexcited singlet electron–hole pair initially forms a pair of correlated electron–hole pairs that eventually dissociates and decoheres into separate electron–hole pairs.^{1–5} The strong electronic correlations present in low-dimensional conjugated molecules means that the exchange energy between the singlet and triplet electron–hole pairs is so large that the singlet energy is approximately twice the triplet energy.⁶ Consequently, the subsequent spin-conserving process of the formation of two electron–hole pairs implies that this is an entangled pair of two triplets in an overall singlet state (also known as a spin-correlated triplet-pair).

In contrast to some other researchers,⁵ in this paper, we explicitly define singlet fission as the process by which a singlet electron–hole pair interconverts to an entangled pair of triplets, which ultimately dissociates and spin-decoheres into two separate, uncorrelated triplets. A quantitative definition of singlet fission will be given in Sec. V C.

Singlet fission has widely been investigated in polyacenes. The work on polyacenes is partly motivated by the observation that the

creation of a pair of electron–hole pairs by a photon of twice the excitation energy of each pair in tandem with a material that produces a single electron–hole pair of the same energy has the potential to exceed the Shockley–Queisser power conversion efficiency limit of ~30%.^{7,8}

In polyacenes, it is widely accepted that the conversion of one electron–hole pair into two correlated electron–hole pairs is a bimolecular process.^{2,9–11} In this case, via a two-electron process, the initial singlet electron–hole pair created on one molecule forms a pair of triplet electron–hole pairs in an overall singlet state that is delocalized over two molecules.

The study of singlet fission in carotenoids and polyenes is at a less mature stage than that in polyacenes.^{3,12,13} In long polyene-type systems, there is evidence of triplet formation via singlet fission on single chains.^{14–16} For shorter polyenes, e.g., carotenoids, however, singlet fission appears only to occur in aggregates and dimers.^{17–26}

There is some controversy about whether or not singlet fission in carotenoid aggregates precedes via an intramolecular singlet triplet-pair intermediate. On the one hand, as for polyacenes, Musser *et al.*²⁰ argued that singlet fission in a variety of carotenoid aggregates proceeds directly from the bright (S_2) state to a bimolec-

ular triplet-pair state. On the other hand, however, Kundu and Dasgupta²² argued that singlet fission in lycopene H-aggregates proceeds via an intramolecular triplet-pair state (which they identify as S^* or $1^1B_u^-$). Similarly, Quaranta *et al.*²³ also observed that singlet fission in lutein/violaxanthin aggregates occurs via an intramolecular intermediate. In this paper, we describe a theory of singlet fission in carotenoid dimers that is explicitly based on the assumption of an intramolecular intermediate triplet-pair state. We now describe the formation and character of these triplet-pair states.

Owing to both strong electron–electron interactions and electron–nuclear coupling, the excited states of polyenes and carotenoids are more complex than those of polyacenes. In particular, the well-known “bright” to “dark” state internal conversion^{27–29} leads to the formation of a highly correlated low-energy state (usually labeled $2A_g$ or S_1).

One possible “bright” to “dark” state internal conversion process in carotenoids is illustrated in Fig. 1. This shows an energy

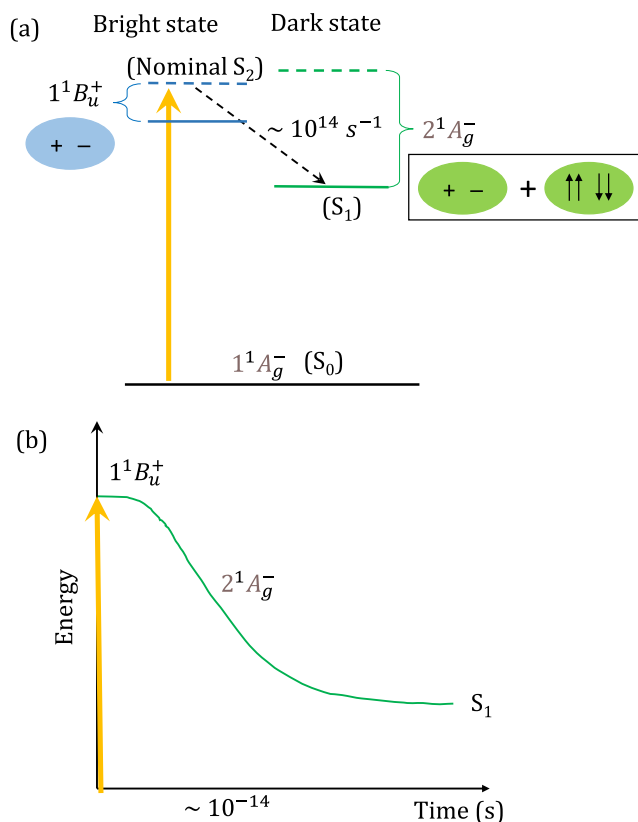


FIG. 1. Schematic diagrams illustrating the internal conversion between the excited “bright” and “dark” states of a carotenoid. (a) Diabatic state representation: $1^1B_u^+$ (blue) and $2^1A_g^-$ (green). The dashed (solid) horizontal lines represent the vertical (relaxed) energies of the states. The approximate rate constant is also indicated. (b) Adiabatic state representation, showing S_1 , evolves adiabatically from the predominately $1^1B_u^+$ state (i.e., a Frenkel exciton) to the predominately $2^1A_g^-$ state (i.e., a linear superposition of a singlet triplet-pair and an odd-parity charge-transfer exciton). (Internal conversion from the $1^1B_u^+$ to $2^1A_g^-$ state via the intermediate $1^1B_u^-$ state is illustrated in Fig. 4 of Ref. 28.)

level crossing between the diabatic $1^1B_u^+$ and $2^1A_g^-$ states, occurring within 10 fs of photoexcitation as a consequence of strong electron–nuclear coupling.²⁸ In an adiabatic representation,³⁰ the S_1 state, initially predominately the $1^1B_u^+$ state, exhibits an *avoided crossing* with the S_2 state, initially predominately the $2^1A_g^-$ state, such that after 10 fs, S_1 becomes predominately the $2^1A_g^-$ state. However, this is not the only possible “bright” to “dark” state internal conversion process.^{27,28,31,32} This is because the $2^1A_g^-$ state is just the lowest-energy member of a band (or family) of “ $2A_g$ ” states,³³ namely, states of the same fundamental excitation with different center-of-mass pseudomomenta, i.e., $2^1A_g^-$, $1^1B_u^-$, and $3^1A_g^-$. Thus, another internal conversion process from the $1^1B_u^+$ to $2^1A_g^-$ state is via the intermediate $1^1B_u^-$ state. These two processes are described in detail in Refs. 27–29.

We now turn to a more detailed discussion of the “ $2A_g$ ” family of states. As shown in Refs. 28, 33, and 34, these states are a linear superposition of a singlet triplet-pair and an odd-parity charge-transfer exciton [as schematically illustrated in Fig. 1(a)]. The hybridization between these two components causes a strong triplet–triplet attraction.³⁴ It also implies that the energy of the $2^1A_g^-$ state is ~ 0.4 eV lower than the energy of a pair of noninteracting triplets on a chain of the same length.³³ Thus, intrachain singlet fission from the $2^1A_g^-$ state is a strongly endothermic process (although it becomes less endothermic and potentially exothermic from higher energy members of the “ $2A_g$ ” family^{27,33}—a point that we return to in the Conclusions).

As already mentioned, singlet fission in polyacenes is an intrinsically bimolecular process. However, the triplet-pair character of the $2^1A_g^-$ state of polyenes suggests that for these systems, the initial step of the formation of an entangled triplet-pair is an intrinsically unimolecular process. In this paper, we focus on singlet fission from the $2^1A_g^-$ state. Owing to strong endothermic intrachain dissociation for this state, we propose that the second step toward energetically favorable singlet fission is a bimolecular mechanism. In Ref. 28, a possible mechanism of bimolecular exothermic dissociation was suggested. This mechanism relies on the additional vibrational and torsional reorganization energies that a pair of individual triplets on separate chains gains over a pair of bound triplets on the same chain. It thus assumes that carotenoids are in a twisted configuration in their ground state and planarize in their excited states.

In this paper, we introduce a minimal model of triplet-pair dissociation and decoherence in carotenoid dimers. We start by assuming that the $2^1A_g^-$ state formed via an internal conversion on a single chain is entirely composed of a correlated singlet triplet-pair. The triplets on a single chain interact with one another and delocalize along the chain via a superexchange mechanism. A triplet may also hop onto a neighboring chain, thereby losing its triplet-pair interaction. However, by doing so, it gains an offset (or driving) energy from the additional reorganization energies discussed in the previous paragraph.

In order to understand the singlet fission process, we compute various metrics. We distinguish between bound, intrachain singlet triplet-pairs and noninteracting, interchain triplet-pairs, and we compute their populations. Since the dynamics and equilibrium properties are ultimately determined by the energy spectrum of the quantum system, we discuss the single and double chain spectra in some detail. We model the dynamics of the open quan-

tum system using the quantum Liouville equation in which both spin-conserving and spin interconversion dephasing processes are included.

The plan of this paper is as follows: In Sec. II, we introduce and motivate our model (a fuller justification is given in Appendix A). Section III describes the singlet, triplet, and quintet triplet-pair spectrum of the single and coupled chain Hamiltonians. Section IV describes our computational methodology and introduces the key metrics by which we investigate the singlet fission process. (Appendix B discusses whether two measures of quantum entanglement correctly describe fission of the entangled triplet-pair.) We present and discuss both our dynamical and equilibrium results in Sec. V. We conclude and outline proposals for future work in Sec. VI.

II. MODEL OF TRIPLET-PAIR STATES

A. The triplet-pair basis

Our model for the triplet-pair states of carotenoids and polyenes is based on the valence bond model of strongly correlated systems,³⁵ as illustrated in Fig. 2. The ground state is shown by the chain labeled $\times = 2$. Each p_z orbital is singly occupied, while both electrons on an ethylene dimer form a singlet bond. A triplet excitation on the i th dimer is denoted as $|0; i\rangle$ or $|\pm 1; i\rangle$, for the $M_s = 0$ or $M_s = \pm 1$ spin-projections, respectively. A pair of triplet excitations on dimers i and j is shown for the chain labeled $\times = 1$ in Fig. 2.

As described in the Introduction, we assume that within tens of fs, the photoexcited Frenkel exciton undergoes an internal conversion to a singlet triplet-pair state on a single chain (e.g., $\times = 1$). The initial entangled pair is, thus,

$$^1|\Phi(t=0)\rangle = \sum_{ij \in \times=1} \Phi_{ij}(t=0) |i, j\rangle, \quad (1)$$

where the singlet triplet-pair basis state is

$$^1|i, j\rangle = \frac{1}{\sqrt{3}} (|1; i\rangle - |1; j\rangle - |0; i\rangle|0; j\rangle + |-1; i\rangle|1; j\rangle). \quad (2)$$

For the initial state $^1|\Phi(t=0)\rangle$, i and j label the dimers in chain $\times = 1$. However, for a general eigenstate of the full two-chain Hamiltonian (introduced in Sec. II B), i and j can label dimers on separate chains.

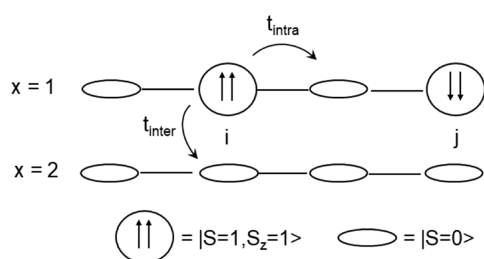


FIG. 2. A schematic illustration of a carotenoid dimer with a triplet-pair on chain $\times = 1$, with triplets on ethylene dimers i and j . The chain $\times = 2$ is in its ground state. t_{intra} and t_{inter} are the hopping matrix elements between neighboring intrachain and interchain ethylene dimers, respectively.

A pair of triplets within the valence bond basis is coupled to form an overall singlet, triplet, or quintet state. In this work, we investigate the role of transverse spin-dephasing that connects the $S_z = 0$ components of each total spin. The $S_z = 0$ components of the triplet and quintet triplet-pair bases are

$$^3|i, j\rangle = \frac{1}{\sqrt{2}} (|1; i\rangle|1; j\rangle - |-1; i\rangle|1; j\rangle) \quad (3)$$

and

$$^5|i, j\rangle = \frac{1}{\sqrt{6}} (|1; i\rangle|1; j\rangle + 2|0; i\rangle|0; j\rangle + |-1; i\rangle|1; j\rangle), \quad (4)$$

respectively.

B. The two-chain Hamiltonian

Assuming the valence bond model approximation, the low-energy physics of carotenoids and polyenes are then described by the spin-1/2 Heisenberg antiferromagnet. As described in more detail in Appendix A, within the reduced triplet-pair basis introduced above, the Heisenberg antiferromagnet for a pair of chains reduces to the following Hamiltonian:

$$\hat{H} = \sum_{\times=1,2} \hat{H}_{\text{single}}^{\times} + \hat{H}_{\text{double}} + \hat{H}_{\text{inter}}. \quad (5)$$

$\hat{H}_{\text{single}}^{\times}$ is the intrachain Hamiltonian for a pair of triplets on the same chain, \times ,

$$\begin{aligned} \hat{H}_{\text{single}}^{\times=1,2} = & 2E_T \sum_{i,j \in \times} |i, j\rangle\langle i, j| + t_{\text{intra}} \sum_{i \neq j \in \times} (|i \pm 1, j\rangle\langle i, j| \\ & + \text{H.C.}) - V \sum_{i \in \times} |i, i+1\rangle\langle i, i+1|. \end{aligned} \quad (6)$$

The first term on the right-hand side describes the excitation of a pair of triplets on dimers i and j on the same chain, while the second term describes the hopping of triplets between neighboring dimers on the same chain. The final term describes the spin-dependent exchange interaction between a pair of triplets on neighboring dimers. The origin of this interaction is explained in Appendix A. This interaction may also be written as³⁶

$$J \hat{S}_i^{(1)} \cdot \hat{S}_{i+1}^{(1)}, \quad (7)$$

where $\hat{S}^{(1)}$ is the spin-1 (triplet) operator and J is the *inter*-triplet exchange interaction. Thus, the singlet and triplet triplet-pairs experience a nearest-neighbor attraction, $V_S = +2J$ and $V_T = +J$, respectively, while the quintet triplet-pair experiences a nearest-neighbor repulsion $V_Q = -J$.

\hat{H}_{double} is the intrachain Hamiltonian for a pair of triplets on separate chains,

$$\begin{aligned} \hat{H}_{\text{double}} = & 2(E_T - \varepsilon) \sum_{i \in \times=1} \sum_{j \in \times=2} |i, j\rangle\langle i, j| \\ & + t_{\text{intra}} \sum_{i \in \times=1} \sum_{j \in \times=2} [(|i \pm 1, j\rangle\langle i, j| + \text{H.C.}) + (|i, j \pm 1\rangle\langle i, j| + \text{H.C.})]. \end{aligned} \quad (8)$$

The first term on the right-hand side describes the excitation of a pair of triplets on dimers i and j on different chains. ε is the offset energy that each triplet gains because of the additional reorganization energy that each separate triplet gains over a bound pair on

the same chain. The second and third terms describe the hopping of triplets between neighboring dimers on the same chain.

Finally, \hat{H}_{inter} is the interchain Hamiltonian that couples both chains,

$$\hat{H}_{\text{inter}} = t_{\text{inter}} \sum_{\mathbf{x}=1}^2 \sum_{i_{\mathbf{x}}} \sum_{j_{\mathbf{x}} > i_{\mathbf{x}}} [(|i_{\mathbf{x}}, j_{\mathbf{x}}\rangle \langle i_{\mathbf{x}}, j_{\mathbf{x}}| + \text{H.C.}) + (|i_{\mathbf{x}}, j_{\mathbf{x}}\rangle \langle i_{\mathbf{x}}, j_{\mathbf{x}}| + \text{H.C.})], \quad (9)$$

where $i_{\mathbf{x}}$ and $j_{\mathbf{x}}$ mean the i th dimer on opposite chains. This describes the hopping of triplets between the nearest neighbor dimers of both chains, as illustrated in Fig. 2.

III. THE TRIPLET-PAIR STATES AND SPECTRUM

Here, we describe the single and double chain triplet-pair spectra, as this helps explain the dynamics of singlet fission.

A. The single-chain spectrum

The solution of the two-particle single chain Hamiltonian \hat{H}_{single} , Eq. (6), is well-known.^{37–39} In a chain with periodic boundary conditions, there is a triplet-pair correlated state, which we denote as $|TT\rangle$, which forms a band with energy

$$E_k^{\text{bound}} = (2E_T - V) - \frac{4t_{\text{intra}}^2}{V} \cos^2(k/2), \quad (10)$$

where k is the dimensionless wavevector, satisfying $-\pi \leq k \leq \pi$. Similarly, the energy of a pair of free, noninteracting triplets, which we denote as $|T \cdots T\rangle$, is

$$E_k^{\text{free}} = 2E_T - 4t_{\text{intra}} \cos(k). \quad (11)$$

Thus, the binding energy of the triplet-pair correlated state on a single chain is

$$\begin{aligned} \text{BE}_{\text{single}} &= (E_{k=0}^{\text{free}} - E_{k=0}^{\text{bound}}) \\ &= V + \frac{4t_{\text{intra}}^2}{V} - 4|t_{\text{intra}}|. \end{aligned} \quad (12)$$

This result implies that the triplet-pair is bound if V exceeds the critical value, $V_c = 2|t_{\text{intra}}|$.

These predictions remain qualitatively correct for linear chains with open boundary conditions, although V_c decreases for shorter chains, as shown in Fig. 12 of Appendix A.

Figure 3 illustrates the single-chain spectrum of the singlet triplet-pair. Assuming that $V_S > V_c$, the band of bound states, labeled $|TT\rangle$, form the “ $2A_g$ ” family of states (i.e., $2^1A_g^-, 1^1B_u^-, 3^1A_g^-, \dots$). The noninteracting but spin-correlated pairs form the $|T \cdots T\rangle$ band.

Owing to the large gap between the lowest $|TT\rangle$ state and the band of $|T \cdots T\rangle$ state, we find that the latter are never populated during the dynamics and so we no longer consider them.

B. The double-chain spectrum

We define $|T \cdots T\rangle_{1-2}$ as a noninteracting, interchain singlet triplet-pair eigenstate of the double chain Hamiltonian \hat{H}_{double} , Eq. (8).

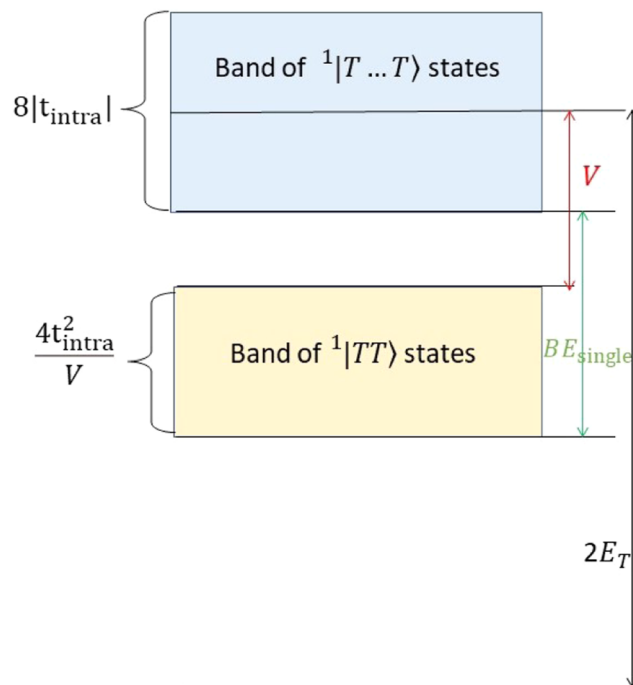


FIG. 3. Spectrum of the intrachain singlet triplet-pair states, as determined by Eqs. (10) and (11). $|TT\rangle$ are bound intrachain singlet triplet-pairs, which form the “ $2A_g$ ” family of states (i.e., $2^1A_g^-, 1^1B_u^-, 3^1A_g^-, \dots$). $|T \cdots T\rangle$ are unbound intrachain singlet triplet-pairs. The triplet-pairs are bound if $V > V_c = 2|t_{\text{intra}}|$. (An equivalent description applies to triplet triplet-pairs. In contrast, the quintet triplet-pairs are antibound.) Compare with the inset of Fig. 12 that shows the energy levels of triplet-pairs on a pair of ethylene dimers.

For finite-length and open uncoupled chains, the energy to dissociate a singlet triplet-pair on a single chain (i.e., $|TT\rangle$) into two noninteracting triplets on separate chains (i.e., $|T \cdots T\rangle_{1-2}$) is defined by

$$\text{BE} = E_{\text{double}}(\varepsilon = 0) - E_{\text{single}}(V > V_c), \quad (13)$$

where E_{single} and E_{double} are the lowest singlet energies of \hat{H}_{single} and \hat{H}_{double} , respectively. This binding energy is smaller than the binding energy on a single chain because of the quantum deconfinement of single triplets on separate chains. For example, when $V_S = 2.8t_{\text{intra}}$ and for 20 C-sites on each chain, $\text{BE} = 0.3272t_{\text{intra}}$, whereas $\text{BE}_{\text{single}} = 0.5637t_{\text{intra}}$.

The triplet and quintet triplet-pair eigenstates of \hat{H}_{double} are the noninteracting, interchain pairs, denoted as $|T \cdots T\rangle_{1-2}$ and $|T \cdots T\rangle_{1-2}$, respectively. These states are degenerate with $|T \cdots T\rangle_{1-2}$.

C. The full two-chain spectrum

We now discuss the spectrum of the full two-chain Hamiltonian, given by Eq. (5). Since single triplets on separate chains each

gain an offset potential energy of ε , bound, intrachain singlet triplet-pairs and noninteracting, interchain triplet-pairs are degenerate when $2\varepsilon = BE$. We will denote this as the “degeneracy point.”

For uncoupled chains (i.e., $t_{\text{inter}} = 0$) when $\varepsilon < BE/2$, the lowest singlet eigenstate is a linear superposition of $^1|TT\rangle_1$ and $^1|TT\rangle_2$. In this regime, singlet fission is endothermic. Conversely, when $\varepsilon > BE/2$, the lowest singlet eigenstate is $^1|T \cdots T\rangle_{1-2}$ and singlet fission is exothermic.

Coupling the two chains via \hat{H}_{inter} causes $^1|TT\rangle$ and $^1|T \cdots T\rangle_{1-2}$ to hybridize. In general, the singlet triplet-pair eigenstates of the full two-chain Hamiltonian are a linear combination of the intra- and interchain pair states, i.e.,

$$^1|\Psi\rangle = \frac{a}{\sqrt{2}}(^1|TT\rangle_1 \pm ^1|TT\rangle_2) + b^1|T \cdots T\rangle_{1-2}. \quad (14)$$

The lowest energy singlet eigenstate is predominately composed of $^1|TT\rangle_1$ and $^1|TT\rangle_2$ in the endothermic regime (i.e., $|a|^2 > |b|^2$) and predominately composed of $^1|T \cdots T\rangle_{1-2}$ in the exothermic regime (i.e., $|a|^2 < |b|^2$), as illustrated in Fig. 4(b).

As an example, consider the low-energy singlet triplet-pair spectrum at the degeneracy point, $\varepsilon = BE/2$. Denoting the degenerate trio of (diabatic) singlet triplet-pair states as $^1|TT\rangle_1 \equiv |1\rangle$, $^1|T \cdots T\rangle_{1-2} \equiv |2\rangle$, and $^1|TT\rangle_2 \equiv |3\rangle$, the interchain coupling causes these states to hybridize to form the eigenstate $^1|\Psi_j\rangle = \frac{1}{2} \sum_n \sin(\pi j n / 4) |n\rangle$ ($j = 1, 2, 3$). In particular, the bonding eigenstate $^1|\Psi_{j=1}\rangle = (|1\rangle + \sqrt{2}|2\rangle + |3\rangle)/2$ is lower in energy by $\Delta \propto t_{\text{inter}}$ from the non-bonding eigenstate, $^1|\Psi_{j=2}\rangle = (|1\rangle + |3\rangle)/\sqrt{2}$. This energy gap determines the time-period of the coherent triplet-pair population oscillations described in Sec. V A.

Next, let us consider the relative energies of the lowest singlet, triplet, and quintet triplet-pair eigenstates of the full two-chain Hamiltonian. As discussed in Sec. III B, when $t_{\text{inter}} = 0$ and $\varepsilon = 0$, the singlet triplet-pair is bound on a single chain with a binding energy, BE , given by Eq. (13). In contrast, because of weaker intrachain exchange interactions, the triplet and quintet triplet-pair eigenstates are the noninteracting, interchain pairs, $^3|T \cdots T\rangle_{1-2}$ and $^5|T \cdots T\rangle_{1-2}$, respectively. Thus, when $t_{\text{inter}} = 0$ and $\varepsilon = 0$, the binding energy, BE , is equal to the exchange energy, ΔE_S , which separates the interacting singlet triplet-pair from the noninteracting, interchain triplet and quintet triplet-pairs. As the offset energy, ε , increases, the interchain pair energies decrease. When $t_{\text{inter}} = 0$, $\Delta E_S = (BE - 2\varepsilon)$, which vanishes at the degeneracy point and in the exothermic regime. ΔE_S is illustrated schematically in Fig. 4(a) and is shown as a function of ε when $t_{\text{inter}} = 0$ as the dashed line in Fig. 4.

As we have seen, when the chains are coupled, the intra- and interchain singlet triplet-pairs hybridize to give the singlet eigenstate, Eq. (14). In contrast, the triplet and quintet triplet-pair eigenstates remain predominately interchain in character. This means that the exchange energy, ΔE_S , increases with t_{inter} because the intrachain triplet-triplet attraction causes an effective interchain triplet-triplet attraction in the singlet state. This is illustrated for two values of t_{inter} in Fig. 4.

Notice that since the quintet interchain triplet-pairs are noninteracting, ΔE_S is also the energy to dissociate the singlet triplet-pair

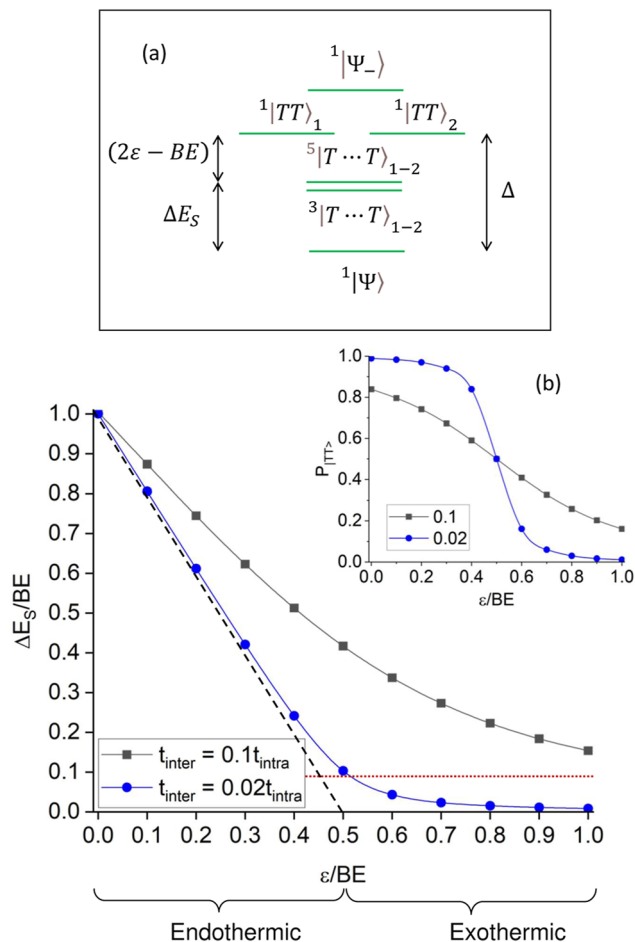


FIG. 4. Two-chain exchange energy, ΔE_S , vs the offset-energy, ε , for weak and intermediate interchain coupling, t_{inter} . ΔE_S , illustrated in inset (a), is the energy gap between the lowest energy singlet triplet-pair eigenstate, $^1|\Psi\rangle$, of the full two-chain Hamiltonian and the interchain quintet triplet-pair state, $^5|T \cdots T\rangle_{1-2}$. The black dashed-line shows $\Delta E_S(t_{\text{inter}} = 0) = (BE - 2\varepsilon)$, where BE [Eq. (13)] is the energy to dissociate an intrachain singlet triplet-pair into two noninteracting, interchain triplets in the limit $t_{\text{inter}} = 0$. $\varepsilon < BE/2$ ($\varepsilon > BE/2$) corresponds to endothermic (exothermic) singlet fission when $t_{\text{inter}} = 0$. The red horizontal dashed-line represents the value of $k_B T$ at $T = 300$ K. $t_{\text{intra}} = 0.88$ eV. Also shown in inset (a) are the intrachain triplet-pair states, $^1|TT\rangle$, the interchain triplet triplet-pair state, $^3|T \cdots T\rangle_{1-2}$, the antibonding counterpart to Eq. (14), i.e., $^1|\Psi_-\rangle$, and the energy gap, Δ , that determines the coherent oscillations described in Sec. V A 1. Inset (b) shows the probability that the lowest singlet eigenstate, $^1|\Psi\rangle$, occupies $^1|TT\rangle$, i.e., $P_{1111} \equiv |a|^2$.

eigenstate into a pair of noninteracting triplets on separate chains, defined by

$$\Delta E_S = E(V = 0, \varepsilon, t_{\text{inter}}) - E(V > V_c, \varepsilon, t_{\text{inter}}), \quad (15)$$

where E is the lowest singlet energy of \hat{H} . Thus, in the presence of spin-dephasing, when $\Delta E_S \lesssim k_B T$, the $^1|T \cdots T\rangle_{1-2}$, $^3|T \cdots T\rangle_{1-2}$,

and $^5|T \cdots T\rangle_{1-2}$ states mix to become uncorrelated, noninteracting single triplets on each chain. Figure 4 shows the value of $k_B T$ when $T = 300$ K. For weak interchain coupling (i.e., $t_{\text{inter}} = 0.02t_{\text{intra}}$), ΔE_S is smaller than $k_B T$ in the exothermic regime.

Figure 4(a) shows a schematic energy level diagram of the key triplet-pair states involved in singlet fission.

IV. THEORETICAL AND COMPUTATIONAL METHODOLOGY

A. The quantum Liouville equation

The nonequilibrium dynamics of the quantum system is fully described by its time-dependent density operator, whose time-evolution is determined by the quantum Liouville equation. We compute the evolution of the density operator in the eigenstate basis of the two-chain Hamiltonian, i.e., $\rho_{ab} = \langle a|\hat{\rho}|b\rangle$. In this work, we adopt the frequently used secular approximation,^{40,41} which explicitly decouples the evolution of the populations (i.e., the diagonal elements of the density matrix) from the coherences (i.e., the off-diagonal elements of the density matrix).

For spin-conserving processes arising from nonmagnetic system–bath interactions, the quantum Liouville equation for the populations $P_a \equiv \rho_{aa}$ is

$$\frac{dP_a}{dt} = -\sum_{b \neq a} (k_{ab}P_a - k_{ba}P_b), \quad (16)$$

while for the coherences, it is

$$\frac{d\rho_{ab}}{dt} = -i\omega_{ab}\rho_{ab} - 2\Gamma_{ab}(1 - \delta_{ab})\rho_{ab}. \quad (17)$$

Defining the Bohr frequencies as $\omega_{ab} = (E_a - E_b)/\hbar$ and taking $\omega_{ab} \geq 0$, the thermal rates are^{40,41}

$$k_{ab} = \left(\frac{2\lambda}{\hbar}\right) J(\omega_{ab}) (n(\omega_{ab}) + 1) C_{ab} \quad (18)$$

and

$$k_{ba} = \left(\frac{2\lambda}{\hbar}\right) J(\omega_{ab}) n(\omega_{ab}) C_{ab}, \quad (19)$$

where $n(\omega) = (\exp \beta \hbar \omega - 1)^{-1}$ is the Bose distribution function and $J(\omega) = \omega \omega_0 / (\omega^2 + \omega_0^2)$ is the (dimensionless) Debye-spectral function.

We note that the thermal rates satisfy detailed balance, i.e., $k_{ba}/k_{ab} = \exp(-\beta \hbar \omega_{ab})$, ensuring that the steady-state eigenstate populations satisfy the Boltzmann distribution. λ is the bath reorganization energy, while $C_{ab} = 2 \sum_m S_{ma} S_{mb}$, where \mathbf{S} is the matrix whose columns are the eigenvectors of the two-chain Hamiltonian represented in the “site” basis. $2\Gamma_{ab} = (\gamma_a + \gamma_b)$, where $\gamma_a = \sum_b k_{ab}$.

We also include magnetic system–bath interactions, induced, for example, by electron–nuclear magnetic dipole interactions. We will consider spin-dephasing from static interactions. This causes transverse relaxation and spin interconversion, i.e., total S_z is conserved, but total S^2 is not. We supplement the quantum Liouville equation with a Lindblad dissipator,^{42,43} where the Lindblad operator acting on each electron is $\hat{L} = \hat{S}_z/\hbar$. The action of

\hat{S}_z on a down-spin reverses its phase;⁴³ thus, our choice of Lindblad operator connects the singlet and quintet states to triplet states.

Using the $S_z = 0$ triplet-pair basis states, we derive the additional population equations of motion as

$$\frac{dP_a^S}{dt} = -\frac{2\gamma}{3} \sum_{b \in T} (k_{ab}P_a^S - k_{ba}P_b^T), \quad (20)$$

$$\frac{dP_a^T}{dt} = -\frac{2\gamma}{3} \sum_{b \in S} (k_{ab}P_a^T - k_{ba}P_b^S) - \frac{\gamma}{3} \sum_{b \in Q} (k_{ab}P_a^T - k_{ba}P_b^Q), \quad (21)$$

and

$$\frac{dP_a^Q}{dt} = -\frac{\gamma}{3} \sum_{b \in T} (k_{ab}P_a^Q - k_{ba}P_b^T). \quad (22)$$

Here, P_a^S , P_a^T , and P_a^Q are the populations of eigenstate $|a\rangle$ in the singlet, triplet, and quintet spin-sectors, respectively. In order to maintain detailed balance, the rates k_{ab} and k_{ba} are given by Eqs. (18) and (19). However, γ is a multiplicative factor to account for the different strengths of the magnetic and nonmagnetic interactions. In this work, we have taken $\gamma = 10^{-3}$.

The initial condition on the density operator is that $\hat{\rho}(0) = |^1\Phi(0)\rangle\langle^1\Phi(0)|$, where $|^1\Phi(0)\rangle$ is the lowest-energy singlet eigenstate of the single-chain Hamiltonian for chain $x = 1$, Eq. (6), i.e., it is the lowest energy member of the band of intrachain singlet triplet-pair states, $^1|TT\rangle_1$, described in Sec. III A.

B. Observables

In order to understand the singlet fission process, we calculate various observables. These are as follows:

- Eigenstate and site basis coherences, defined, respectively, as

$$C_{\text{eigenstate}} = \sum_{ab} |\rho_{ab}| - 1 \quad (23)$$

and

$$C_{\text{site}} = \sum_{mm'} |\tilde{\rho}_{mm'}| - 1, \quad (24)$$

where m denotes the basis state $|ij\rangle$.

- Triplet-pair populations, $P_\alpha(t)$, in a projected subspace, α , defined as

$$P_\alpha(t) = \text{Tr} \{ \hat{P}_\alpha \hat{\rho}(t) \}, \quad (25)$$

where the projection operator is

$$\hat{P}_\alpha = \sum_{ij \in \alpha} |ij\rangle\langle ij|. \quad (26)$$

Here, the projected sub-spaces of interest are the singlet, triplet, and quintet pair-subspaces, as well as the additional projection of these subspaces onto a single or double chain. These projections allow us to identify the populations of the intrachain triplet-pair states, $^1|TT\rangle_1$ and $^1|TT\rangle_2$, and the interchain triplet-pair states, $^{2S+1}|T \cdots T\rangle_{1-2}$, with a definite spin, S .

- The expectation value of the total spin,

$$\begin{aligned}\langle S^2 \rangle &= \text{Tr} \{ \hat{S}^2 \hat{\rho} \} \\ &= \hbar^2 (0 \times P_S + 2 \times P_T + 6 \times P_Q).\end{aligned}\quad (27)$$

At complete singlet fission, $P_S = P_T = P_Q = 1/3$ (for S_z conserving spin-dephasing) and $\langle S^2 \rangle = 8\hbar^2/3$.

C. Numerical techniques

The decoupling of populations and coherences via the secular approximation considerably reduces the complexity of solving the quantum Liouville equation. This is a significant advantage, as even for this reduced basis model, the Hilbert space of this problem is large.

The population equations of motion, Eq. (16), can be cast into the general form

$$\frac{dP_a}{dt} = \sum_{\forall b} K_{ab} P_b, \quad (28)$$

where \mathbf{K} is the matrix of the rate constants. The solution from linear algebra is

$$P_a(t) = \sum_{bc} S_{ab} \exp(\lambda_b t) S_{bc}^{-1} P_c(0), \quad (29)$$

where \mathbf{S} is the matrix whose columns are the eigenvectors of \mathbf{K} , $\{\lambda\}$ are the corresponding eigenvalues, and $P_c(0)$ is an initial condition.

Equation (17) has the simple solution

$$\rho_{ab}(t) = \rho_{ab}(0) \exp((-i\omega_{ab} - 2\Gamma_{ab})t). \quad (30)$$

D. Parameters

The intrachain triplet hopping matrix element, t_{intra} , can be estimated via the Pariser–Parr–Pople (or extended Hubbard) model of π -conjugated systems.⁶ The intrachain triplet hopping between ethylene dimers is a second-order process, occurring via a virtual charge-transfer state. According to Ref. 34, the superexchange transfer integral is $t_{\text{intra}} = -\alpha^2 \beta_s^2 / \Delta_{\text{CT}}$, where Δ_{CT} is the energy gap to the virtual charge-transfer triplet state, β_s is the one-electron transfer integral across a single bond (≈ 2.2 eV), and α^2 is the probability that the neighboring singlet dimer is in the covalent state (shown as a lozenge in Fig. 2). Using Pariser–Parr–Pople model parameters, we estimate t_{intra} to be ~ 0.88 eV.³⁴

The interchain triplet hopping is also a two-electron virtual process. The values of the one-electron interchain transfer integrals depend sensitively on interchain separations and conformation. According to Ref. 13, for decapentaene monomers in a H-dimer separated by 3.55 Å, the interdimer one-electron transfer integrals are ~ 0.4 eV. However, since one-electron transfer integrals decay as $\exp(-r\xi)$, where⁴⁴ $\xi = 3.07 \text{ \AA}^{-1}$, a small increase in separation to 4.0 Å reduces this coupling to 0.1 eV. Similarly, a rotated dimer or a mixed H-J dimer has a typical coupling value of 0.1 eV (see Fig. 4 of Ref. 13 for further details). Reference 10 cites one-electron transfer integrals for polyacene dimers of order 0.1 eV. The intradimer one-electron transfer integral is $2.2/2 = 1.1$ eV. Thus, the interdimer one-electron transfer integrals are ~ 3 – 10 times smaller than

the corresponding intrachain value. This implies that the interchain superexchange is ~ 10 – 100 times smaller than the intrachain superexchange, and thus, we take t_{inter} as a variable, satisfying $0.1t_{\text{intra}} \leq t_{\text{inter}} \leq 0.01t_{\text{intra}}$.

As shown in Appendix A, according to the valence-bond model, the singlet triplet-pair exchange interaction is $V_S = 2J = 2t_{\text{intra}}$. As also discussed in Sec. III A and shown in Fig. 12, this would imply that the triplet-pair is not bound in polyenes, an observation at variance with experiment²⁶ and rigorous DMRG calculations.³³ This discrepancy is a consequence of using the reduced valence-bond basis, which has no ionic contributions.³⁴ However, as it is theoretically and computationally expedient to use this minimal basis, we account for the discrepancy by treating V_S as an adjustable parameter. We thus set $V_S = 2.8t_{\text{intra}}$, which (as shown in Fig. 12) reproduces the binding energy derived from the enlarged valence-bond-exciton basis.³⁴

It is difficult to predict definitive values for the driving potential, ε . Using the results of Ref. 28, we find that for a pair of twisted carotenoid chains of 20 atoms each, with a ground state twist of 15° and a rotational constant of $K_{\text{rot}} = 8 \text{ eV rad}^{-2}$, triplet-pair dissociation is exothermic with an energy of ~ 32 meV. This implies that $\varepsilon/\text{BE} = 0.55$.

We set the reorganization energy to a value typical of conjugated molecular systems,¹⁰ namely $\lambda = 0.05$ eV, and there are 20 C-atoms per chain. For convenience, the adjustable and derived parameters are listed in Table I.

E. Glossary of terms

For convenience, Table II contains a list of terms and definitions used in this paper. In particular, it defines the different types of triplet-pair states that are the subject of Sec. V.

V. RESULTS AND DISCUSSION

We now turn to discuss our results, starting with a discussion of the dynamics of the triplet-pairs, before describing how the model parameters determine their equilibrium populations. We summarize our findings in Sec. V C.

A. Dynamics

All the dynamical simulations were computed at the degeneracy point, i.e., $\varepsilon = \text{BE}/2$, with $t_{\text{inter}} = 0.02t_{\text{intra}}$ and $t_{\text{intra}} = 0.88$ eV, and at a temperature $T = 300$ K.

TABLE I. Values of parameters used in this paper. (See also Table II.)

Parameter	Value
t_{intra} , Eq. (6)	0.88 eV
No. of C-atoms per chain, N	20
$\text{BE}_{\text{single}}$	$0.5637t_{\text{intra}} = 0.50$ eV
BE	$0.3272t_{\text{intra}} = 0.29$ eV
Singlet triplet-pair attraction, $V_S = 2J$, Eq. (5)	$2.8t_{\text{intra}} = 2.46$ eV
Reorganization energy, λ	0.05 eV
Temperature, T	300 K

TABLE II. A glossary of terms and definitions used in this paper.

Term	Definition
t_{intra}	The intrachain triplet hopping matrix element.
t_{inter}	The interchain triplet hopping matrix element.
$J = V_S/2$	The intrachain triplet–triplet exchange interaction.
ε	The interchain triplet offset energy. $2\varepsilon < \text{BE}$ ($2\varepsilon > \text{BE}$) implies potential endothermic (exothermic) singlet fission in the limit that $t_{\text{inter}} = 0$.
$^1 TT\rangle_{\times}$	A bound, <i>intrachain</i> singlet triplet-pair localized on chain \times . $^1 TT\rangle$ is an eigenstate of the single chain Hamiltonian \hat{H}_{single} , Eq. (6).
$^{2S+1} T \cdots T\rangle_{1-2}$	A noninteracting, <i>interchain</i> triplet-pair with spin S . $^{2S+1} T \cdots T\rangle_{1-2}$ is an eigenstate of the double chain Hamiltonian \hat{H}_{double} , Eq. (8).
$^1 \Psi\rangle$	Singlet eigenstate of the full two-chain Hamiltonian [Eq. (5)], defined in Eq. (14).
$ T\rangle_{\times}$	A single triplet localized on chain \times .
$\text{BE}_{\text{single}}$	The energy to dissociate the lowest energy $^1 TT\rangle$ state into two non-interacting <i>intrachain</i> triplets. It is defined by Eq. (12) and is illustrated in Fig. 3. Notice that since triplets in the quintet pair state are unbound, $\text{BE}_{\text{single}}$ is also the intrachain singlet-quintet triplet-pair exchange energy.
BE	The energy to dissociate the lowest energy $^1 TT\rangle$ state into two noninteracting, <i>interchain</i> triplets in the limit that $t_{\text{inter}} = \varepsilon = 0$. It is defined by Eq. (13).
ΔE_S	The exchange energy between the lowest energy singlet triplet-pair eigenstate [Eq. (14)] of the full two-chain Hamiltonian [Eq. (5)] and the noninteracting, <i>interchain</i> quintet state, $^5 T \cdots T\rangle_{1-2}$. ΔE_S is also the energy to dissociate the lowest energy singlet triplet-pair eigenstate into two noninteracting, <i>interchain</i> triplets for general t_{inter} and ε . [Note that $\Delta E_S(\varepsilon=0, t_{\text{inter}}=0) \equiv \text{BE}$.] It is defined by Eq. (15) and is shown in Fig. 4.

1. Unitary evolution of the closed quantum system

We begin our discussion of the dynamics by investigating the triplet-pair populations in the unitary limit, i.e., when the evolution is only determined by the time-dependent Schrödinger equation for a closed system. Figure 5 illustrates the coherent oscillations of the triplet-pair populations at the degeneracy point, $\varepsilon = \text{BE}/2$. The initial $^1|TT\rangle_1$ population on chain 1 transfers to chain 2 via the interchain $^1|T \cdots T\rangle_{1-2}$ state. At 33 fs, $P(^1|T \cdots T\rangle_{1-2}) = 0.5$, while $P(^1|TT\rangle_1) = P(^1|TT\rangle_2) = 0.25$. At 66 fs, the triplet-pair population has entirely transferred to chain 2. The return probability period, τ [i.e., the period for which $P(^1|TT\rangle_1) = 1$], is 132 fs. This period is determined by the energy gap between the bonding and nonbonding two-chain singlet triplet-pair eigenstates, discussed in Sec. III C, i.e., by $\Delta \propto t_{\text{inter}}$ and, thus, $\tau \propto 1/t_{\text{inter}}$.

Associated with the coherent population dynamics are oscillations in the site-coherence as illustrated in Fig. 6. As expected, the

site coherence is maximized when $P(^1|T \cdots T\rangle_{1-2})$ is maximized and $P(^1|TT\rangle)$ are minimized.

2. The role of dissipation

We now turn to the role of thermal dissipation in the absence of spin-dephasing. Again, Fig. 7 shows the triplet-pair populations as a function of time at the degeneracy point. Comparing the inset of Fig. 7 with Fig. 5, we see that after each return period, τ , the $^1|T \cdots T\rangle_{1-2}$ population accumulates, while the net $^1|TT\rangle$ population decreases. The oscillations of these populations are damped, reaching equilibrated values of $P(^1|TT\rangle) \sim 0.6$ and $P(^1|T \cdots T\rangle_{1-2}) \sim 0.4$ within 5 ps.

The coherences are displayed in Fig. 8. As expected from Eq. (30), the eigenstate coherence decreases as a sum of exponentials; a single-exponential fit gives a decay time ~ 1 ps. The eigenstate coherences are negligible after 5 ps, meaning that population of the

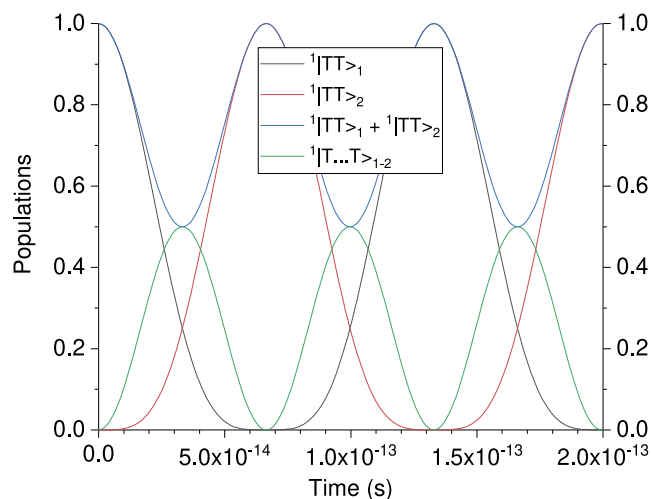


FIG. 5. Coherent oscillations of the triplet-pair populations in the absence of dephasing. Here, the time-period of the return probability [i.e., $P(1|TT)_1 = 1$] is $\tau \propto 1/t_{\text{inter}}$. (See also Fig. 6.)

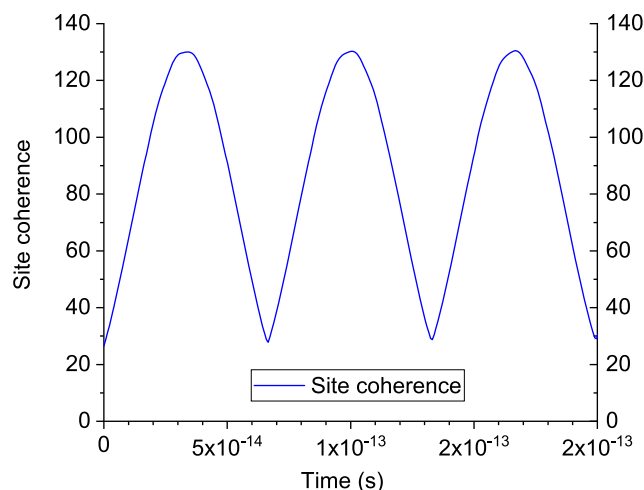


FIG. 6. Oscillations of the site-coherence in the absence of dephasing. This is maximized when the inter-chain population, $1|T \cdots T\rangle_{1-2}$, is maximized. (See also Fig. 5.)

eigenstates of the full two-chain Hamiltonian have achieved their (classical) Boltzmann values. The oscillations of the site-coherence are damped, again reaching steady-state values within 5 ps. The time-averaged site-coherence increases monotonically, from 76 to 94, indicating that this is not a good measure of the “quantumness” of the entangled pair.

Some authors define the creation of a population of $1|T \cdots T\rangle_{1-2}$ states as singlet fission,⁵ partly because for some spec-

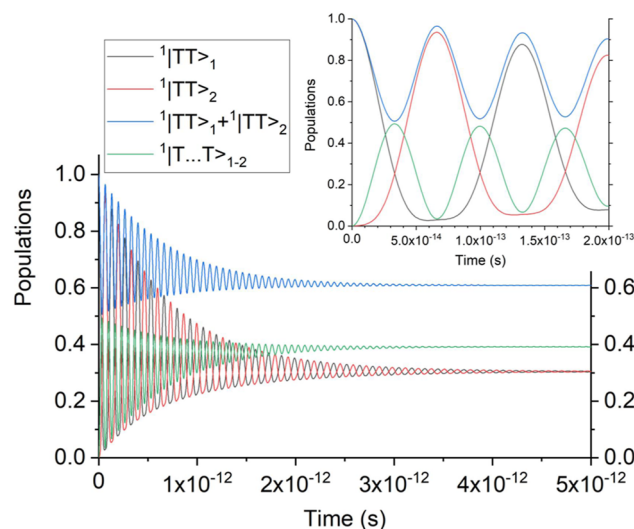


FIG. 7. Populations as a function of time without spin-dephasing of the intrachain singlet triplet-pair states, $1|TT\rangle_1$ and $1|TT\rangle_2$, and the interchain singlet triplet-pair state, $1|T \cdots T\rangle_{1-2}$. The populations have thermalized within 5 ps. The inset shows the ultrafast population dynamics.

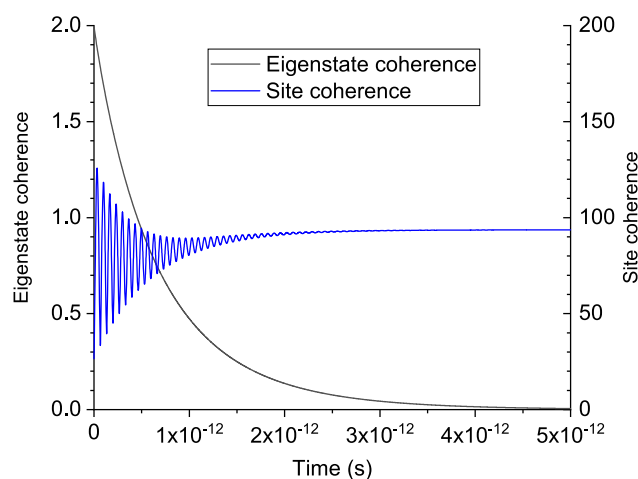


FIG. 8. Site and eigenstate coherences as a function of time. The decay time of the eigenstate coherence is ~ 1 ps.

troscopies, spin-correlated but noninteracting triplet-pairs are indistinguishable from individual triplets.^{3,5} However, from a theoretical perspective, this definition is unsatisfactory as, in general, the $1|T \cdots T\rangle_{1-2}$ component is part of the correlated singlet triplet-pair eigenstate, $1|\Psi\rangle$ [Eq. (14)]. As described in Section III C, it costs an energy ΔE_S to dissociate (i.e., split or divide) this state into separate, uncorrelated triplets. We return to our definition of singlet fission in Sec. V C.

3. The role of spin dephasing

Finally, in our description of the dynamics, we turn to the role of spin-dephasing. To distinguish the kinetics of this process from the spin-conserving thermalization described in Sec. V A 2, we take a spin-dephasing rate 10^{-3} times smaller, implying a spin-relaxation time of ~ 1 ns. Spin-dephasing causes population transfer from the interchain singlet triplet-pairs to the interchain triplet and quintet triplet-pairs, i.e., to the $S_z = 0$ components of $^3|T \cdots T\rangle_{1-2}$ and $^5|T \cdots T\rangle_{1-2}$ from $^1|T \cdots T\rangle_{1-2}$. However, as $^3|T \cdots T\rangle_{1-2}$ and $^5|T \cdots T\rangle_{1-2}$ are quasidegenerate, they are mixed by spin-dephasing, implying that they are equivalent to uncorrelated, single triplets on each chain.

The triplet populations are illustrated in Fig. 9. These results show that after the thermalization of the $^1|TT\rangle$ and $^1|T \cdots T\rangle_{1-2}$ populations in less than 5 ps (at ~ 0.60 and ~ 0.40 , respectively), slower spin-dephasing converts some of the $^1|TT\rangle$ and $^1|T \cdots T\rangle_{1-2}$ population to $^3|T \cdots T\rangle_{1-2}$ and $^5|T \cdots T\rangle_{1-2}$. The equilibrated $^1|TT\rangle$ and $^1|T \cdots T\rangle_{1-2}$ populations are now 0.42 and 0.27, respectively, while the $^3|T \cdots T\rangle_{1-2}$ and $^5|T \cdots T\rangle_{1-2}$ populations are equal and sum to 0.31. We remark that for these parameters, the two-chain exchange energy, ΔE_S , is (just) greater than $k_B T$. Thus, the lowest energy singlet triplet-pair eigenstate [given by Eq. (14)] does not readily interconvert with $^3|T \cdots T\rangle_{1-2}$ and $^5|T \cdots T\rangle_{1-2}$.

The dynamics of singlet fission within the exothermic regime are described in Appendix B.

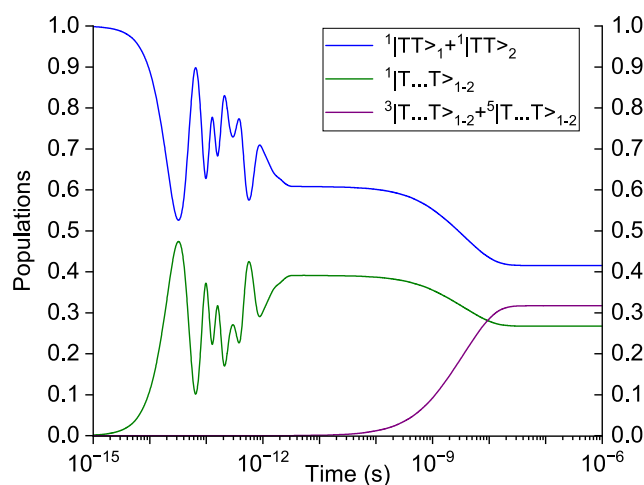


FIG. 9. Populations as a function of time with spin dephasing of the intrachain singlet triplet-pair states, $^1|TT\rangle$, and the interchain singlet triplet-pair state, $^1|T \cdots T\rangle_{1-2}$. Also shown is the joint population of the interchain triplet and quintet triplet-pair states, $^3|T \cdots T\rangle_{1-2}$ and $^5|T \cdots T\rangle_{1-2}$. The spin dephasing rate is 10^{-3} times smaller than the Redfield thermalization rate. These results show that following thermalization of the $^1|TT\rangle_x$ and $^1|T \cdots T\rangle_{1-2}$ populations in less than 5 ps, slower spin-dephasing converts some of the $^1|TT\rangle_x$ and $^1|T \cdots T\rangle_{1-2}$ populations to $^3|T \cdots T\rangle_{1-2}$ and $^5|T \cdots T\rangle_{1-2}$ (or equivalently, $|T\rangle_1$ and $|T\rangle_2$).

B. Equilibrium properties

The time taken for the spin populations to thermally equilibrate evidently depends on the rates of dissipation and dephasing. In this section, we assume that equilibration has occurred and we now discuss the equilibrium populations in order to understand the fate of the initial entangled pair.

Figure 10 illustrates the intrachain singlet triplet-pair, $^1|TT\rangle$, populations as a function of the offset-potential, ϵ , for different t_{inter} . For all our results, the temperature $T = 300$ K. In the $t_{\text{inter}} = 0$ limit, there is an energy-level crossing at $\epsilon = BE/2$ between a singlet eigenstate with triplet-pairs on either chain and one with the triplet-pair separated on both chains. This is illustrated by the dashed step-function in Fig. 10. At $t_{\text{inter}} = 0$, for $\epsilon < BE/2$, the triplet-pair is on either chain 1 or chain 2 and $P(^1|TT\rangle) = 1$. Conversely, for $\epsilon > BE/2$, the triplet-pair is separated on both chains and $P(^1|TT\rangle) = 0$. Furthermore, as shown in Fig. 4, for $\epsilon \geq BE/2$, the exchange energy, ΔE_S , vanishes when $t_{\text{inter}} = 0$. Therefore, if spin-dephasing is present, the singlet, triplet, and quintet interchain triplet-pairs mix, implying complete singlet fission, i.e., $P(|T\rangle) = 2$. However, for $t_{\text{inter}} \neq 0$, there is an avoided crossing at $\epsilon = BE/2$ and the step function is smeared out with increasing t_{inter} , as illustrated in Fig. 10.

The interchain triplet-pair population may also be inferred from Fig. 10, as it is given by $[1 - P(^1|TT\rangle)]$. Depending on the parameter regimes and temperature, this interchain population becomes a mixture of interchain singlet triplet-pairs, $^1|T \cdots T\rangle_{1-2}$, and uncorrelated triplets, $|T\rangle$. We can understand this more fully via Figs. 4 and 11. The solid curves with square symbols in Fig. 11 indicate the $^1|T \cdots T\rangle_{1-2}$ populations as a function of the offset-potential for weak and intermediate (i.e., $t_{\text{inter}} = 0.1 t_{\text{intra}}$) interchain coupling. As

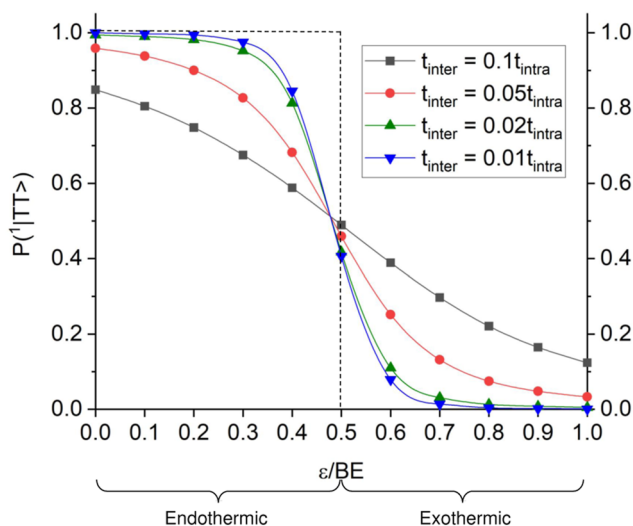


FIG. 10. Equilibrated intrachain singlet triplet-pair, $^1|TT\rangle$, population as a function of the offset-potential, ϵ , for different t_{inter} . The step function, represented by the dashed lines, is the result for $t_{\text{inter}} = 0$, showing that an energy-level crossing occurs at $\epsilon = BE/2$. This becomes an avoided crossing for $t_{\text{inter}} \neq 0$. $\epsilon < BE/2$ ($\epsilon > BE/2$) corresponds to the possible endothermic (exothermic) singlet fission, as explained in Sec. V.

shown in Fig. 4, for intermediate interchain coupling, the exchange energy, ΔE_S , is larger than $k_B T$. Nonetheless, for $\varepsilon > BE/2$, thermal excitation into the triplet and quintet sectors is possible, as indicated by the black dashed curve with circle symbols in Fig. 11. As these states are quasidegenerate, they mix forming single triplets on separate chains.

Conversely, as also shown in Fig. 4, for weak interchain coupling, the exchange energy, ΔE_S , is smaller than $k_B T$ in the exothermic regime ($\varepsilon > BE/2$). In this regime, the singlet, triplet, and quintet interchain pairs mix to form uncorrelated triplets on each chain. This represents complete singlet-fission of the initial $^1|TT\rangle_1$ state and is indicated in Fig. 11 by $P(^1|T \cdots T\rangle_{1-2}) \approx P(^3|T \cdots T\rangle_{1-2}) \approx P(^5|T \cdots T\rangle_{1-2}) \approx 1/3$ at $\varepsilon/BE \gtrsim 0.6$.

C. Singlet fission: The fate of the entangled pair

As described in previous studies,^{33,34} the singlet triplet-pair is one component of the “dark” state of carotenoids, which is born within tens of fs following photoexcitation of the “bright” state. (The other component of the “dark” state is a charge-transfer exciton. Although this has the important role of causing triplet-triplet attraction, it is not relevant to the rest of the present discussion.)

The initial singlet triplet-pair wavefunction is given by Eqs. (1) and (2), indicating that it is an entangled pair of triplets. This paper has described the subsequent fate of this pair, showing that it intricately depends on a range of microscopic parameters and temperature. The two key Hamiltonian parameters are the interchain coupling, t_{inter} , and the potential energy offset, ε . A third parameter, the intrachain coupling t_{intra} , sets the overall energy scale and, hence, determines the timescales of the dynamics. The detailed kinetics of singlet fission depend on the various dissipation and spin-dephasing

parameters, while the final equilibrium populations depend on the Hamiltonian parameters and temperature.

The entangled pair, itself, exists as two components. The first component is the strongly bound *intrachain* pair, $^1|TT\rangle$. As shown in Fig. 5, this pair oscillates between both chains with a time period determined at the degeneracy point by t_{inter} . During this transfer of population, the second component of the entangled pair is created, namely the noninteracting, *interchain* pair, $^1|T \cdots T\rangle_{1-2}$.

In the absence of external dissipation, this nonstationary state dynamics is fully described in Fig. 5. As shown in Fig. 7, however, the spin-conserving thermalization causes a time-averaged population to transfer from $^1|TT\rangle$ to $^1|T \cdots T\rangle_{1-2}$. In general, the thermally equilibrated system will be composed of $^1|TT\rangle$ and $^1|T \cdots T\rangle_{1-2}$. In the absence of spin-dephasing, $^1|T \cdots T\rangle_{1-2}$ retains its spin coherence, and thus, true singlet fission into separate, uncorrelated triplets has not occurred.

To a good approximation, deep within the exothermic regime in the absence of spin interconversion, the system is described by the density operator,

$$\hat{\rho} = ^1|T \cdots T\rangle_{1-2} \langle T \cdots T|_{1-2}, \quad (31)$$

where

$$^1|T \cdots T\rangle_{1-2} = \sum_{i \in \mathbf{x}=1} \sum_{j \in \mathbf{x}=2} \psi_{ij} ^1|i, j\rangle, \quad (32)$$

in which $^1|i, j\rangle$ is defined in Eq. (2), and

$$\psi_i = \left(\frac{2}{N+1} \right)^{1/2} \sum_{i \in \mathbf{x}} (-1)^i \sin \left(\frac{i\pi}{N+1} \right). \quad (33)$$

Thus, within the eigenstate basis, the density matrix has a single (diagonal) entry corresponding to $^1|T \cdots T\rangle_{1-2}$. The absence of coherences within this basis, however, hides the fact that the triplets are still entangled as $^1|i, j\rangle$ cannot be written as the product $|i\rangle \otimes |j\rangle$.

The final step of singlet fission occurs during spin-dephasing. As shown in Fig. 9, spin-dephasing causes population to transfer from $^1|T \cdots T\rangle_{1-2}$ to the interchain triplet and quintet triplet-pair states, i.e., $^3|T \cdots T\rangle_{1-2}$ and $^5|T \cdots T\rangle_{1-2}$, respectively. Since the triplet and quintet triplet-pair states are quasidegenerate, they are mixed by spin-dephasing to form single, uncorrelated triplets on each chain, i.e., $|T\rangle_1$ and $|T\rangle_2$. Assuming that spin-dephasing is slower than thermalization of the $^1|TT\rangle$ and $^1|T \cdots T\rangle_{1-2}$ states, the kinetic scheme is, therefore,⁴⁵

$$^1|TT\rangle \rightarrow ^1|T \cdots T\rangle_{1-2} \rightarrow |T\rangle_1 + |T\rangle_2. \quad (34)$$

Figure 9 shows this separation of timescales in the singlet fission process. Evidently, there are three distinct time regimes. First, for $1 \text{ fs} \lesssim t \lesssim 1 \text{ ps}$, there are coherent oscillations between intra- and interchain singlet triplet-pair states. Second, for $1 \text{ ps} \lesssim t \lesssim 1 \text{ ns}$, there is spin conserving thermalization and population transfer from the intrachain to the interchain singlet triplet-pair states. Finally, for $t \gtrsim 1 \text{ ns}$, there is spin nonconserving dephasing and population transfer from the interchain singlet triplet-pair state to the interchain triplet and quintet triplet-pair states, or equivalently to uncorrelated triplet pairs.

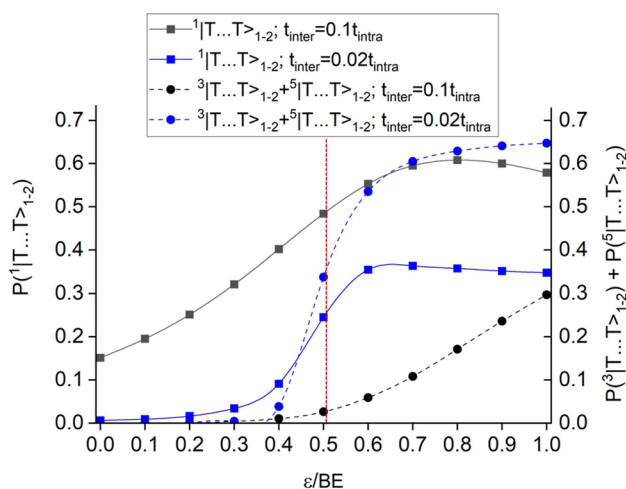


FIG. 11. Equilibrated populations of the interchain singlet triplet-pair state, $^1|T \cdots T\rangle_{1-2}$, and the sum of the populations of the interchain triplet and quintet triplet-pair states, $^3|T \cdots T\rangle_{1-2}$ and $^5|T \cdots T\rangle_{1-2}$, as a function of the offset-potential, ε . The red vertical dashed-line represents the value of ε at which $\Delta E_S = k_B T$ for $t_{\text{inter}} = 0.02 t_{\text{intra}}$. It, therefore, indicates the crossover at which $^1|T \cdots T\rangle_{1-2}$ mixes with $^3|T \cdots T\rangle_{1-2}$ and $^5|T \cdots T\rangle_{1-2}$, which together populate the uncorrelated $|T\rangle_1$ and $|T\rangle_2$ states.

As already mentioned, and as illustrated in Figs. 10 and 11, the equilibrated populations depend on the Hamiltonian parameters and temperature. For weak interchain coupling (i.e., $t_{\text{inter}} \lesssim 0.02t_{\text{intra}}$), there is a relatively sharp singlet-fission transition at the degeneracy point, where for $\varepsilon < \text{BE}/2$ (i.e., the endothermic regime), most of the triplet-pair population is $^1|TT\rangle$, whereas for $\varepsilon > \text{BE}/2$ (i.e., the exothermic regime), the triplets are an equal population of $^1|T \cdots T\rangle_{1-2}$, $^3|T \cdots T\rangle_{1-2}$, and $^5|T \cdots T\rangle_{1-2}$ (or equivalently, $|T\rangle_1$ and $|T\rangle_2$).

Conversely, for stronger interchain coupling (i.e., $t_{\text{inter}} \approx 0.1t_{\text{intra}}$), there is a smoother crossover from predominately $^1|TT\rangle$ population to predominately both $^1|TT\rangle$ and $^1|T \cdots T\rangle_{1-2}$ population to predominately both $^1|T \cdots T\rangle_{1-2}$ and $|T\rangle$ population as ε is increased from the endothermic to exothermic regime.

In conclusion, complete singlet fission of $^1|TT\rangle$ occurs when the populations of the eigenstates $^1|T \cdots T\rangle_{1-2}$, $^3|T \cdots T\rangle_{1-2}$ and $^5|T \cdots T\rangle_{1-2}$ are fully thermalized and equal 1/3 each,⁴⁶ with no coherences between them. Then, the density operator may be expressed as

$$\hat{\rho} = \frac{1}{3} \left(^1|T \cdots T\rangle_{1-2} \langle T \cdots T|_{1-2} + ^3|T \cdots T\rangle_{1-2} \langle T \cdots T|_{1-2} + ^5|T \cdots T\rangle_{1-2} \langle T \cdots T|_{1-2} \right). \quad (35)$$

To illustrate that the triplets are now unentangled, we introduce an alternative representation of the density operator. To this end, we turn to the single-triplet basis states introduced in Sec. II, namely $|M_s; i\rangle$ for a triplet with spin-projection M_s on the i th dimer. The density operator in the singlet-fission limit can now be constructed as follows: First, construct the (spin-uncoupled) triplet-pair product wavefunctions for individual triplets on chains 1 and 2, i.e.,

$$|\Psi_1\rangle = |M_s = +1; \times = 1\rangle |M_s = -1, \times = 2\rangle, \quad (36)$$

$$|\Psi_2\rangle = |M_s = 0; \times = 1\rangle |M_s = 0, \times = 2\rangle, \quad (37)$$

and

$$|\Psi_3\rangle = |M_s = -1; \times = 1\rangle |M_s = +1, \times = 2\rangle, \quad (38)$$

where

$$|M_s; \times\rangle = \sum_{i \in \times} \psi_i |M_s; i\rangle \quad (39)$$

and ψ_i , given in Eq. (33), is the triplet wavefunction delocalized on chain \times . Then, the mixed-state density operator is⁴⁵

$$\hat{\rho} = \frac{1}{3} (|\Psi_1\rangle \langle \Psi_1| + |\Psi_2\rangle \langle \Psi_2| + |\Psi_3\rangle \langle \Psi_3|). \quad (40)$$

Now, the populations of $|T\rangle_1$ and $|T\rangle_2$ are each unity and $\langle S^2 \rangle = 8\hbar^2/3$. This happens, for example, for $t_{\text{inter}} = 0.02t_{\text{intra}}$ deep in the exothermic regime, as shown in Fig. 11 at $\varepsilon = \text{BE}$.

In Appendix B, we further explore the dynamics of singlet fission deep within the exothermic regime. In particular, we investigate whether two numerical measures of pair-entanglement, namely the

Horodecki entanglement and the entanglement entropy, correctly describe the kinetic scheme shown by Eq. (34).

VI. CONCLUDING REMARKS

As described in the Introduction, singlet fission in carotenoids is a multistep process. After photoexcitation, the “bright” state undergoes an ultrafast internal conversion to the “dark” state. The “dark” state (often labeled the S_1 or $2A_g$ state) is a linear combination of an entangled singlet triplet-pair and an odd-parity charge-transfer exciton. By building a minimal model of the triplet-pair component of the “dark” state and using the quantum Liouville equation, this paper has described the subsequent fate of the triplet-pair in a carotenoid dimer. Our key findings are summarized in Sec. V C.

The theory developed in this paper is predicated on the assumption that in carotenoids and polyenes, unlike in polyacenes, the initial step of forming an entangled triplet-pair from the photoexcited electron-hole pair is an intrachain process. However, as just indicated, the “dark” state has some charge-transfer character. Moreover, the initial photoexcited electron-hole pair does not evolve completely into the “dark” state but retains some Frenkel-exciton “bright” state character.^{27,28} Thus, a complete theory of singlet fission in carotenoid systems should include the singlet electron-hole components of the initial state to determine whether there is also bimolecular triplet-pair formation.

This paper has also focused on singlet fission from the lowest member of the “ $2A_g$ ” family of states (i.e., the $2^1A_g^-$ state), for which intrachain singlet fission is strongly endothermic. However, theory^{27,28,33} and experiment^{31,32} both indicate that internal conversion to the 2^1A_g state may occur via intermediate states, i.e., via higher energy members of the “ $2A_g$ ” family of states from which intrachain singlet fission is potentially exothermic.³³ Indeed, Kundu and Dasgupta²² argue from their transient absorption experiments that the $1^1B_u^-$ state is the relevant intramolecular intermediate for singlet fission. Again, this possibility needs to be investigated in further theoretical work.

Using a model Hamiltonian with adjustable parameters, we have been able to explore the “parameter space” of singlet fission in carotenoid dimers, thus understanding the kinetics and predicting the equilibrated yields. However, in order to make concrete predictions to explain experimental observations, we will need to include additional interactions, e.g., spin dipole-dipole interactions and spin-orbit coupling, and to derive *ab initio* parameters for realistic carotenoid conformations. In conclusion, this paper has presented a first step to theoretically model the rich and fascinating physics of singlet fission in carotenoid systems, but there is clearly much more theoretical and computational modeling to do.

ACKNOWLEDGMENTS

We thank Claudia Tait and Max Marcus for helpful discussions.

AUTHOR DECLARATIONS

Conflict of Interest

The authors have no conflicts to disclose.

Author Contributions

William Barford: Conceptualization (lead); Formal analysis (equal); Investigation (equal); Methodology (equal); Project administration (lead); Software (equal); Supervision (lead); Validation (equal); Writing – original draft (lead); Writing – review & editing (lead).
Cameron A. Chambers: Investigation (equal); Software (equal); Validation (equal); Writing – original draft (supporting); Writing – review & editing (supporting).

DATA AVAILABILITY

The data that support the findings of this study are available from the corresponding author upon reasonable request.

APPENDIX A: HEISENBERG MODEL OF TRIPLET-PAIR STATES

The low-energy spin-physics of carotenoids and polyenes is approximately described by the spin-1/2 dimerized Heisenberg antiferromagnet. Its Hamiltonian is

$$\hat{H} = J_d \sum_{n \text{ odd}} \hat{S}_n \cdot \hat{S}_{n+1} + J_s \sum_{n \text{ even}} \hat{S}_n \cdot \hat{S}_{n+1}, \quad (\text{A1})$$

where n labels a p_z orbital on the n th C-atom and \hat{S}_n is the spin-1/2 operator acting on the electron in that orbital. This Hamiltonian can be derived from the underlying Pariser–Parr–Pople model⁶ of π -conjugated systems in the limit that the one-electron transfer integral between neighboring p_z orbitals, β , is much smaller than $(U - V_1)$, where U and V_1 are the onsite and nearest neighbor Coulomb repulsions, respectively. Since $4\beta \simeq U$ in π -conjugated systems, this limit is not strictly valid. However, the Heisenberg antiferromagnet provides a good starting point for describing the low-energy covalent states of π -conjugated systems (and it explains, for example, why the $2^1A_g^-$ state lies lower in energy than the $1^1B_u^+$ state).

J_d and J_s are the superexchange parameters for spin-1/2 electrons across the double and single bonds, respectively. Their origin lies in electron transfer between orbitals via a virtual charge-transfer state, higher in energy by $(U - V_1)$. Thus, they are proportional to $\beta^2/(U - V_1)$.

We assume that the ground state of a carotenoid is a product of singlet dimers located on each double bond. A single triplet excitation corresponds to exciting one of these singlet dimers into a triplet, labeled i , with an excitation energy, $E_T = J_d$. Similarly, a triplet-pair corresponds to two excited singlet dimers, labeled i and j , with an excitation energy $2J_d$. Two triplets can be coupled to form a singlet, triplet, or quintet spin-eigenstate. The $S_z = 0$ components of these states are given in Eqs. (2)–(4).

Rewriting $\hat{S}_n \cdot \hat{S}_{n+1}$ as $(\hat{S}_n^z \hat{S}_{n+1}^z + (\hat{S}_n^+ \hat{S}_{n+1}^- + \hat{S}_n^- \hat{S}_{n+1}^+)/2)$ and using the triplet-pair wavefunctions [Eqs. (2)–(4)], it is easy to show the following:

- Triplets hop across the single-bond between neighboring dimers with a hopping matrix element, $t_{\text{intra}} = -J_s/4$.
- A pair of triplets in an overall singlet eigenstate experiences a nearest neighbor-dimer attraction, $V_S = J_s/2$.
- A pair of triplets in an overall triplet eigenstate experiences a nearest neighbor-dimer attraction, $V_T = J_s/4$.

- A pair of triplets in an overall quintet eigenstate experiences a nearest neighbor-dimer repulsion, $V_Q = -J_s/4$.

The energy levels for a triplet-pair occupying a pair of dimers are shown in the inset of Fig. 12. These relative energy levels may also be obtained by diagonalizing $J\hat{S}_1^{(1)} \cdot \hat{S}_2^{(1)}$, where $\hat{S}^{(1)}$ is the spin-1 (triplet) operator and $J = J_s/4$ is the inter-triplet exchange interaction.³⁶

For our purposes, we are interested in a pair of itinerant, interacting triplets on a chain of ethylene dimers. This two-particle scattering problem has been solved.^{37–39} The key result is discussed in Sec. III A, namely that for an infinite chain, a single bound state exists when $V > 2t_{\text{intra}}$. Thus, the parameters derived from the spin-1/2 Heisenberg antiferromagnet do not predict bound triplet-pairs for an infinite chain, because $V_S = J_s/2 = 2t_{\text{intra}}$.

Since the triplet-pair component of the singlet “dark” state of carotenoids and polyenes is strongly bound, we learn from this analysis that the spin-1/2 antiferromagnet Heisenberg model does not fully describe this state. Instead, the “dark” state of carotenoids is more correctly described as a linear combination of a singlet triplet-pair and a real charge-transfer state. As shown in Ref. 34, it is the hybridization between these two components that causes a stronger attractive interaction (or exchange coupling) between the triplets than that predicted by the pure spin-1/2 Heisenberg model. Figure 12 shows the binding energy of the singlet and triplet triplet-pair states derived from both the Heisenberg model and the model of Ref. 34.

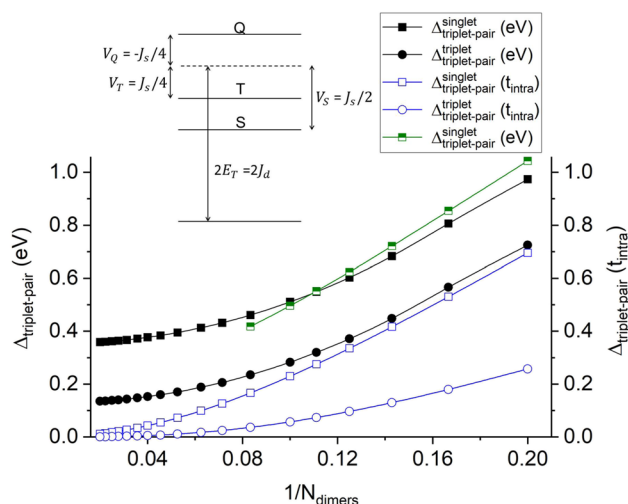


FIG. 12. Binding energies of the singlet and triplet triplet-pair states on a linear chain of N_{dimers} . The results in blue with open symbols are obtained from the one-chain Hamiltonian given in Eq. (6), using parameters derived from the antiferromagnetic Heisenberg model (AFHM), i.e., $V_S = 2t_{\text{intra}}$ and $V_T = t_{\text{intra}}$ (right ordinate). The results in black with filled symbols are obtained from the triplet-pair-charge-transfer-exciton basis model of Ref. 34 (left ordinate). These latter results can be reproduced to a good approximation by Eq. (6) when $V_S = 2.8t_{\text{intra}}$ and $t_{\text{intra}} = 0.88$ eV, as shown by the half-full square symbols in green (left ordinate). The inset shows the singlet, triplet, and quintet triplet-pair energy levels on two dimers, with the spin-1 exchange-interaction parameters determined via the AFHM.

Unfortunately, although still a reduced basis for the many-body problem, the triplet-pair-charge-transfer-exciton basis³⁴ (which itself is a reduced basis version of the exciton-basis valence-bond theory⁴⁷) is too large to perform quantum Liouville simulations for realistic chain lengths. It is, therefore, expedient to retain the minimal valence-bond basis, i.e., of a pair of triplets moving in a chain of singlet dimers but with parameters derived by fitting to the model of Ref. 34. We find that a nearest-neighbor attraction of $V_S = 2.8t_{\text{intra}}$ with $t_{\text{intra}} = 0.88$ eV reproduces the binding energies derived from the model of Ref. 34 shown in Fig. 12.

APPENDIX B: MEASURES OF ENTANGLEMENT

In this appendix, we investigate whether two numerical measures of pair-entanglement, namely the Horodecki entanglement and the entanglement entropy, correctly describe the kinetic scheme shown by Eq. (34).

The Horodecki entanglement^{43,48} of subsystems A and B is defined as

$$E = \log_2 \|(\hat{1}_A \otimes \hat{1}_B) \hat{\rho}_{AB}\|_{\text{tr}}, \quad (\text{B1})$$

where $\|\hat{O}\|_{\text{tr}}$ means the trace norm of \hat{O} (i.e., the sum of the square root of the eigenvalues of $\hat{O}\hat{O}^\dagger$), while $\hat{1}_B$ is the transposition superoperator of subsystem B. Here, we take subsystem A as one component of the triplet-pair, i.e., $A \equiv i$, and subsystem B as the other component, i.e., $B \equiv j$. Thus, the transposition of ρ with respect to j means that $\rho_{(ij)(i'j')} \mapsto \rho_{(ij')(i'j)}$.

The entanglement entropy of subsystems A and B is defined as

$$S = -\sum_{\alpha} \omega_{\alpha} \log_2 \omega_{\alpha}, \quad (\text{B2})$$

where $\{\alpha\}$ are the eigenvalues of the reduced density matrix for subsystem A obtained by tracing over the degrees of freedom of subsystem B. Again, we take $A \equiv i$ and $B \equiv j$. Thus, the reduced density matrix for triplet labeled i is

$$\rho_{ii}^R = \sum_j \rho_{(ij)(i'j)}. \quad (\text{B3})$$

In both cases, we compute the full density matrix in the basis of the spin-uncoupled representation, i.e., $|1, i\rangle|1, j\rangle$, $|0, i\rangle|0, j\rangle$, and $|-1, i\rangle|1, j\rangle$.

We investigate the predictions of these measures of entanglement deep within the exothermic regime, where full singlet fission occurs. We set the spin-dephasing rate so that this is preceded by full interconversion from $^1|TT\rangle$ to $^1|T \cdots T\rangle_{1-2}$. Figure 13 illustrates this dynamics, where we have set $\varepsilon = 1.0 \times \text{BE}$, $t_{\text{inter}} = 0.01t_{\text{intra}}$, and $\gamma = 10^{-3}$.

By ~ 0.1 ns, we observe that there is essentially complete conversion from $^1|TT\rangle$ to $^1|T \cdots T\rangle_{1-2}$, as the population of $^1|T \cdots T\rangle_{1-2} \approx 1$. Although at this time the triplets are still spin-correlated and the value of $\langle S^2 \rangle \approx 0$, the Horodecki entanglement has vanished. Conversely, the entanglement entropy has reached its asymptotic value of ~ 1.6 .

The next process to occur is spin-dephasing and thus, interconversion from $^1|T \cdots T\rangle_{1-2}$ to $^3|T \cdots T\rangle_{1-2}$ and $^5|T \cdots T\rangle_{1-2}$. At 10 ns, the populations of all three equal $1/3$ and $\langle S^2 \rangle = 8\hbar^2/3$, corresponding to complete singlet fission (as described in Sec. V C).

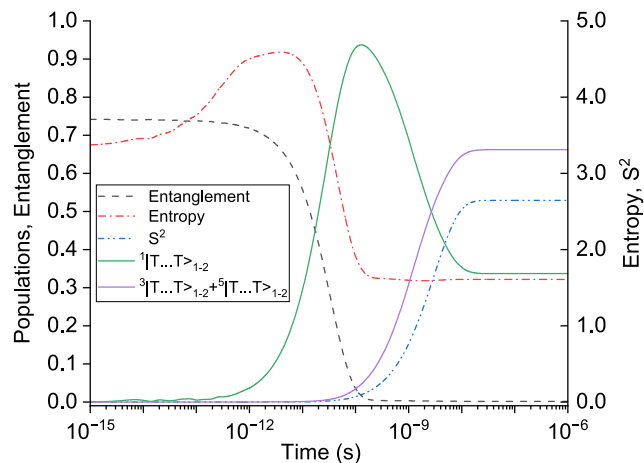


FIG. 13. Dynamics of singlet fission deep within the exothermic regime showing the interchain triplet-pair populations, and the values of the Horodecki entanglement, the entanglement entropy, and $\langle S^2 \rangle / \hbar^2$. $\varepsilon = 1.0 \times \text{BE}$, $t_{\text{inter}} = 0.01t_{\text{intra}}$, and the spin-dephasing coefficient is $\gamma = 10^{-3}$.

However, the values of the Horodecki entanglement and the entanglement entropy remain the same as before. Thus, we find that the Horodecki entanglement vanishes when the system is still entangled, while the entanglement entropy remains finite when the system is no longer entangled. Thus, neither correctly describes the kinetic scheme shown by Eq. (34). We therefore conclude that the only true (albeit proxy) measure of entanglement is the physical observable of the total-spin.

REFERENCES

- M. B. Smith and J. Michl, "Singlet fission," *Chem. Rev.* **110**, 6891–6936 (2010).
- D. Casanova, "Theoretical modeling of singlet fission," *Chem. Rev.* **118**, 7164–7207 (2018).
- A. J. Musser and J. Clark, "Triplet-pair states in organic semiconductors," *Annu. Rev. Phys. Chem.* **70**, 323 (2019).
- S. N. Sanders, A. B. Pun, K. R. Parenti, E. Kumarasamy, L. M. Yablon, M. Y. Sfeir, and L. M. Campos, "Understanding the bound triplet-pair state in singlet fission," *Chem* **5**, 1988 (2019).
- K. Miyata, F. S. Conrad-Burton, F. L. Geyer, and X. Y. Zhu, "Triplet pair states in singlet fission," *Chem. Rev.* **119**, 4261–4292 (2019).
- W. Barford, *Electronic and Optical Properties of Conjugated Polymers*, 2nd ed. (Oxford University Press, Oxford, 2013).
- R. T. Ross and J. M. Collins, "Efficiency of quantum-utilizing solar energy converters in the presence of recombination losses," *J. Appl. Phys.* **51**, 4504–4507 (1980).
- M. C. Hanna and A. J. Nozik, "Solar conversion efficiency of photovoltaic and photoelectrolysis cells with carrier multiplication absorbers," *J. Appl. Phys.* **100**, 074510 (2006).
- T. C. Berkelbach, M. S. Hybertsen, and D. R. Reichman, "Microscopic theory of singlet exciton fission. I. General formulation," *J. Chem. Phys.* **138**, 11410210 (2013).
- T. C. Berkelbach, M. S. Hybertsen, and D. R. Reichman, "Microscopic theory of singlet exciton fission. II. Application to pentacene dimers and the role of superexchange," *J. Chem. Phys.* **138**, 11410310 (2013).
- K. Aryanpour, A. Shukla, and S. Mazumdar, "Theory of singlet fission in polyenes, acene crystals, and covalently linked acene dimers," *J. Phys. Chem. C* **119**, 6966–6979 (2015).

- ¹²H. Kim and P. M. Zimmerman, "Coupled double triplet state in singlet fission," *Phys. Chem. Chem. Phys.* **20**, 30083–30094 (2018).
- ¹³S. Santra, J. Ray, and D. Ghosh, "Mechanism of singlet fission in carotenoids from a polyene model system," *J. Phys. Chem. Lett.* **13**, 6800–6805 (2022).
- ¹⁴B. Kraabel, D. Hulin, C. Aslangul, C. Lapersonne-Meyer, and M. Schott, "Triplet exciton generation, transport and relaxation in isolated polydiacetylene chains: Subpicosecond pump-probe experiments," *Chem. Phys.* **227**, 83 (1998).
- ¹⁵G. Lanzani, S. Stagira, G. Cerullo, S. De Silvestri, D. Comoretto, I. Moggio, C. Cuniberti, G. F. Musso, and G. Dellepiane, "Triplet exciton generation and decay in a red polydiacetylene studied by femtosecond spectroscopy," *Chem. Phys. Lett.* **313**, 525 (1999).
- ¹⁶A. J. Musser, M. Al-Hashimi, M. Maiuri, D. Brida, M. Heeney, G. Cerullo, R. H. Friend, and J. Clark, "Activated singlet exciton fission in a semiconducting polymer," *J. Am. Chem. Soc.* **135**, 12747 (2013).
- ¹⁷C. Wang and M. J. Tauber, "High-yield singlet fission in a zeaxanthin aggregate observed by picosecond resonance Raman spectroscopy," *J. Am. Chem. Soc.* **132**, 13988–13991 (2010).
- ¹⁸C. Wang, D. E. Schlaming, V. Desai, and M. J. Tauber, "Triplet excitons of carotenoids formed by singlet fission in a membrane," *Chemphyschem* **12**, 2891–2894 (2011).
- ¹⁹M. T. Trinh, Y. Zhong, Q. S. Chen, T. Schiros, S. Jockusch, M. Y. Sfeir, M. Steigerwald, C. Nuckolls, and X. Y. Zhu, "Intra- to intermolecular singlet fission," *J. Phys. Chem. C* **119**, 1312–1319 (2015).
- ²⁰A. J. Musser, M. Maiuri, D. Brida, G. Cerullo, R. H. Friend, and J. Clark, "The nature of singlet exciton fission in carotenoid aggregates," *J. Am. Chem. Soc.* **137**, 5130 (2015).
- ²¹M. J. Llansola-Portoles, K. Redekas, S. Streckaite, C. Iliaia, A. A. Pascal, A. Telfer, M. Vengris, L. Valkunas, and B. Robert, "Lycopene crystalloids exhibit singlet exciton fission in tomatoes," *Phys. Chem. Chem. Phys.* **20**, 8640–8646 (2018).
- ²²A. Kundu and J. Dasgupta, "Photogeneration of long-lived triplet states through singlet fission in lycopene H-aggregates," *J. Phys. Chem. Lett.* **12**, 1468–1474 (2021).
- ²³A. Quaranta, A. Krieger-Liszka, A. A. Pascal, F. Perreau, B. Robert, M. Vengris, and M. J. Llansola-Portoles, "Singlet fission in naturally-organized carotenoid molecules," *Phys. Chem. Chem. Phys.* **23**, 4768–4776 (2021).
- ²⁴K. J. Fallon, N. Sawhney, D. T. W. Toolan, A. Sharma, W. X. Zeng, S. Montanaro, A. Leventis, S. Dowland, O. Millington, D. Congrave, A. Bond, R. Friend, A. Rao, and H. Bronstein, "Quantitative singlet fission in solution-processable dithienohexatrienes," *J. Am. Chem. Soc.* **144**, 23516–23521 (2022).
- ²⁵O. Millington, S. Montanaro, A. Leventis, A. Sharma, S. A. Dowland, N. Sawhney, K. J. Fallon, W. X. Zeng, D. G. Congrave, A. J. Musser, A. K. Rao, and H. Bronstein, "Soluble diphenylhexatriene dimers for intramolecular singlet fission with high triplet energy," *J. Am. Chem. Soc.* **145**, 2499–2510 (2023).
- ²⁶G. A. Sutherland, J. P. Pidgeon, H. K. H. Lee, M. S. Proctor, A. Hitchcock, S. Wang, D. Chekulaev, W. C. Tsoi, M. P. Johnson, C. N. Hunter, and J. Clark, "Twisted carotenoids do not support efficient intramolecular singlet fission in the orange carotenoid protein," *J. Phys. Chem. Lett.* **14**, 6135 (2023).
- ²⁷D. Manawadu, D. J. Valentine, M. Marcus, and W. Barford, "Singlet triplet-pair production and possible singlet-fission in carotenoids," *J. Phys. Chem. Lett.* **13**, 1344 (2022).
- ²⁸D. Manawadu, T. N. Georges, and W. Barford, "Photoexcited state dynamics and singlet fission in carotenoids," *J. Phys. Chem. A* **127**, 1342 (2023).
- ²⁹D. Manawadu, D. J. Valentine, and W. Barford, "Dynamical simulations of carotenoid photoexcited states using density matrix renormalization group techniques," *J. Phys. Chem. A* **127**, 3714 (2023).
- ³⁰The "diabatic" $1^1B_u^+$ and $2^1A_g^-$ states are eigenstates of a model Hamiltonian, which assumes that carotenoids possess C_2 and particle-hole symmetry. In contrast, the "adiabatic" S_1 and S_2 states are eigenstates of a model Hamiltonian, which assumes that carotenoids do not possess C_2 and particle-hole symmetry.²⁸
- ³¹H. A. Frank, R. Z. B. Desamero, V. Chynwat, R. Gebhard, I. van der Hoef, F. J. Jansen, J. Lugtenburg, D. Gosztola, and M. R. Wasielewski, "Spectroscopic properties of spheroidene analogs having different extents of π -electron conjugation," *J. Phys. Chem. A* **101**, 149–157 (1997).
- ³²D. Kosumi, K. Yanagi, R. Fujii, H. Hashimoto, and M. Yoshizawa, "Conjugation length dependence of relaxation kinetics in β -carotene homologs probed by femtosecond Kerr-gate fluorescence spectroscopy," *Chem. Phys. Lett.* **425**, 66–70 (2006).
- ³³D. J. Valentine, D. Manawadu, and W. Barford, "Higher-energy triplet-pair states in polyenes and their role in intramolecular singlet fission," *Phys. Rev. B* **102**, 125107 (2020).
- ³⁴W. Barford, "Theory of the dark state of polyenes and carotenoids," *Phys. Rev. B* **106**, 035201 (2022).
- ³⁵C. A. Coulson, *Valence*, 2nd ed. (Oxford University Press, 1961).
- ³⁶C. Kollmar, "Electronic structure of diradical and dicarbene intermediates in short-chain polydiacetylene oligomers," *J. Chem. Phys.* **98**, 7210–7228 (1993).
- ³⁷D. C. Mattis, *The Theory of Magnetism* (Springer-Verlag, Berlin, 1988).
- ³⁸F. B. Gallagher and S. Mazumdar, "Excitons and optical absorption in one-dimensional extended Hubbard models with short- and long-range interactions," *Phys. Rev. B* **56**, 15025 (1997).
- ³⁹F. Gebhard, K. Born, M. Scheidler, P. Thomas, and S. W. Koch, "Exact results for the optical absorption of strongly correlated electrons in a half-filled Peierls-distorted chain," *Philos. Mag. B* **75**, 13 (1997).
- ⁴⁰A. Nitzan, *Chemical Dynamics in Condensed Phases: Relaxation, Transfer and Reactions in Condensed Molecular Systems*, Oxford Graduate Texts (Oxford University Press, Oxford, 2006).
- ⁴¹O. Kühn, *Charge and Energy Transfer Dynamics in Molecular Systems* (Wiley VCH, Weinheim, 2011).
- ⁴²H.-P. Breuer and F. Petruccione, *The Theory of Open Quantum Systems* (Oxford University Press, Oxford, 2002).
- ⁴³M. Marcus and W. Barford, "Triplet-triplet decoherence in singlet fission," *Phys. Rev. B* **102**, 035134 (2020).
- ⁴⁴R. S. Mulliken, C. A. Rieke, D. Orloff, and H. Orloff, "Overlap integrals and chemical binding," *J. Chem. Phys.* **17**, 510 (1949).
- ⁴⁵G. D. Scholes, "Correlated pair states formed by singlet fission and exciton-exciton annihilation," *J. Phys. Chem. A* **119**, 12699–12705 (2015).
- ⁴⁶For the case of pure spin-dephasing and thus conserved S_z .
- ⁴⁷M. Chandross, Y. Shimoi, and S. Mazumdar, "Diagrammatic exciton-basis valence-bond theory of linear polyenes," *Phys. Rev. B* **59**, 4822 (1999).
- ⁴⁸R. Horodecki, P. Horodecki, M. Horodecki, and K. Horodecki, "Quantum entanglement," *Rev. Mod. Phys.* **81**, 865–942 (2009).